Representation of Land-Atmosphere Coupling Processes Over Africa in CMIP6 Models

Anthony Mwanthi (mmwanthi@gmail.com)
University of Nairobi https://orcid.org/0000-0002-0365-374X
Joseph Mutemi
University of Nairobi
Ellen Dyer
University of Oxford
Rachel James
University of Bristol
Franklin Opijah
University of Nairobi
Thomas Webb
University of Oxford
Francis Mutua
University of Nairobi
Richard Washington
University of Oxford
Catherine Senior
Met Office
Segele Zewdu
IGAD Climate Prediction and Applications Centre
Guleid Artan
IGAD Climate Prediction and Applications Centre

Research Article

Keywords: soil moisture, latent heat flux, land-atmosphere coupling, Africa, CMIP6, model

Posted Date: January 3rd, 2022

DOI: https://doi.org/10.21203/rs.3.rs-1139508/v1

Version of Record: A version of this preprint was published at Climate Dynamics on March 2nd, 2023. See the published version at https://doi.org/10.1007/s00382-023-06710-0.

Abstract

Climate models are useful tools that aid in short to long term prediction of the evolution of climate. In this study we assess how CMIP6 models represent coupling between processes over the land and atmosphere, based on terrestrial and atmospheric indices, to show the nature and strength of the coupling relative to the ERA5 datasets over Africa, with a particular focus on the March-May season. Characterization of the annual cycle indicates that model biases are highest during the peak of the rainfall season, and least during the dry season, while soil moisture biases correspond with rainfall amounts. Models show appreciable sensitivity to regional characteristics; there was model consensus in representing East Africa as a limited soil moisture regime, while major differences were noted in the wet regime over Central Africa. Most CMIP6 models tend to over-estimate the strength of the terrestrial and atmospheric pathways over East and Southern Africa. Inter-model differences in coupling indices could be traced to their inter-annual variability rather than to the mean biases of the variables considered. These results are good indicators towards scientific advancement of land surface schemes in the next generation of climate models for better applications in Africa.

1. Introduction

The influence of the land surface on the global climate is important especially at sub-seasonal to seasonal timescales (Dirmeyer, 2011). Soil moisture ‘memory’ is a key factor that can be utilized to enhance the predictability of the regional climate (Koster et al., 2011). Land-atmosphere interactions have specific signatures over different areas around the globe, presenting the opportunity to evaluate the robustness of the current generation of climate models participating in the sixth phase of the Climate Model Intercomparison Project (CMIP6), across various climate regimes. As models gain more prominence in supporting decision making for various socio-economic applications (Lee et al., 2017), it is paramount to evaluate key processes not only as a basis for model improvements, but also inform users on the uncertainty levels associated with climate model outputs (Merchant et al., 2017). Although model development may be a preserve for scientists, information on land surface forcing to the climate is an aspect that societies can appreciate based on their land use practices.

Projected future land cover and land use changes (LCLUC), primarily driven by deforestation, are foreseen to reduce vegetation cover in Africa, South America, eastern Australia and Indonesia (Quesada et al., 2018). Land surface conditions, specifically vegetation and soil moisture have been demonstrated to modify climate extremes such as heat waves (Findell et al., 2017). As humans interact with the biosphere, especially through LCLUCs, there is potential to influence key processes that control the climate. By driving LCLUCs, certain climate forcings are generated through direct changes in land characteristics such as soil moisture, albedo and evapotranspiration that modulate local to regional climate (Betts and Dias, 2010). Hurt et al (2006) noted that human activity has impacted at least 50% of the global land mass, with 25% of global forests cleared within the last three centuries. Consequently, results by Davin and de Noblet-Ducoudré, (2010) indicate that global deforestation yields cooling in high latitudes, induced by changes in snow and albedo, while warming the tropics.

Earlier results based on CMIP3 indicated model consensus in depicting reducing global trends of soil moisture, except for the northern hemisphere winter latitudes (Dirmeyer et al., 2013). Utilizing CMIP5, Lorenz et al., (2016) and Ukkola et al., (2018) noted that decline in soil moisture is expected to amplify temperature extremes. Over Australia, Hirsch et al., (2014) noted that control of soil moisture is important for daily maximum temperatures. However, models over-estimated the land-atmospheric coupling processes erroneously enhancing the temperature extremes (Ukkola et al., 2018). With global temperatures on the increase, it is important that processes that control temperature trends are well simulated in models. In this regard, characterization of land-atmosphere coupling in CMIP6 is important to gauge the robustness of the current generation of climate models.

Existing research suggests that land-atmosphere 'hotspots' are usually located in typical semi-arid regions with pronounced convective rainfall events (Zheng et al., 2015). Such areas have abundant radiation but limited soil moisture. Anomalies in soil moisture trigger latent heat anomalies with corresponding decline in sensible heat resulting in cooling and moistening of the boundary layer (Hohenegger, 2020). Convection may be enhanced or suppressed depending on the pre-existing thermodynamic conditions. The feedback loop is noted where precipitation modulating the land surface states, such as soil moisture (Muller et al., 2020) enhance or diminish the pre-existing processes.

The Global Land–Atmosphere Coupling Experiment (Koster et al., 2006), the Global Soil Wetness Project (Dirmeyer, 2011), and the Project for Intercomparison of Land Surface Parameterization Schemes (PILSPS), (Liang and Guo, 2003) are key initiatives that provided ground-breaking results on land-atmosphere (L-A) processes. The Local Land–Atmosphere Coupling (LoCo) project, (Santanello et al., (2018)) an initiative of Global Energy and Water Exchanges Project- Global Land–Atmosphere System Study, (GEWEX-GLASS) has advanced the L-A studies by developing a set of metrices that aid in characterizing the processes involved in L-A coupling. Observational data, including soil, vegetation and atmospheric characteristics are required for proper characterization of L-A processes and evaluating models. The Land Surface, Snow and Soil Moisture Model Intercomparison Project (LS3MIP), a subexperiment within CMIP6, provides crucial outputs to characterize the influence of the land surface in Earth System Models (ESMs) based on controlled land surface modules (Hurt et al., 2016). Comprehensive field campaigns, such as that carried out in the southern Great Plains of the US by Wulfmeyer et al., (2018), are lacking in many regions, especially over Africa and even on a global scale. There is general lack of long-term observations for land-atmosphere process hence the reliance on model outputs and reanalysis datasets (Dirmeyer et al., 2013).

L-A processes have been shown to influence regional climate in Africa. Over the Sahel, Nicholson (2001) noted that the strong meridional gradient in soil moisture between the Sahara and west Africa regions sustains regional temperature gradients that initiate the development of the African Easterly Jet (AEJ) (Cook, 1999). Klein and Taylor (2020) also noted that soil moisture anomalies enhance the development of both local and propagating convective storms in this region. Feedbacks between the land and atmosphere, especially where soil moisture anomalies sustain rainfall events are related with inter-annual rainfall persistence in the Sahel (Nicholson, 2000). Based on CORDEX-Africa for CMIP5, Soares et al.,

(2019) indicated that the Sahel hotspot of land-atmosphere coupling is projected to increase southwards, due to expected increase in aridity in West Africa.

Over East Africa, loss of vegetation due to human activities as well as climate variability, such as prolonged droughts, have been identified to increase land surface temperatures (Abera et al., 2018). The study further noted that land surface characteristics such as leaf area index and soil moisture explained about 47% of the temporal variability in surface temperatures. On the intra-seasonal timescales in Southern Africa, Dirmeyer at al., (2009) noted that soil moisture memory persisted up to about 40 days. Experimental results by Cook et al (2005) indicated that during the rainfall season in Southern Africa, increase in soil moisture sets in a negative feedback through the partitioning of the surface energy budget; increasing the evaporative fraction triggers surface cooling that creates a high surface pressure and a stable atmosphere.

This paper evaluates the characteristics of coupling between the land and the atmosphere in Africa for selected global models participating in CMIP6. The historical simulations are considered, to provide opportunity for assessment against re-analysis products. Herein, we trace the land-atmosphere coupling processes through the impact of soil moisture characteristics on latent heat fluxes at the land surface, and the consequent impact of surface fluxes to the lower boundary atmosphere conditions, 2-metre temperature. These are usually defined as the terrestrial and atmospheric pathways of the land-atmosphere interactions (Santanello et al., 2018). The structure of the subsequent sections of the paper is as follows; Section 2 presents the Data and Methods, followed by discussion of results in Section 3 and finally, the Conclusions in Section 4.

2. Data And Methods

2.1 Data

The data sources used in this study are European Centre for Medium range Forecasting (ECMWF) version 5 Reanalysis (ERA5), (Hersbach et al., 2020), selected CMIP6 models (Eyring et al., 2016), and Global Inventory Modeling and Mapping Studies (GIMMS) (Zhu et al., 2013). The variables considered are the leaf area index (LAI), soil moisture (SM), rainfall, evapotranspiration and latent heat flux (HFLS).

Most regions across Africa lack long term observations relevant for detailed study of the regional climate as well as model evaluation (Aloysius et al., (2016), Crowhurst et al., (2020)). In this regard, satellite observations as well as reanalysis datasets are best suited to evaluate land-atmosphere characteristics in models (Miralles et al., 2012). Global monthly reanalysis data at 0.25 degree resolution, ERA5, produced by the Copernicus Climate Change Service (C3S) of the European Centre of Medium Range Forecasting (ECMWF) was sourced from the Copernicus Climate Data Store (CDS). ERA5 has better representation of land surface variables such as soil moisture and vegetation over the previous version, ERA-Interim, Hersbach et al., (2020). Global Inventory Modeling and Mapping Studies (GIMMS) monthly mean LAI, LAI3g version 2, climatology at 0.25 degree spatial resolution for the period 1981-2015 was sourced from

the Oak Ridge National Laboratory Distributed Active Archive Center (ORNL DAAC) by the National Aeronautics and Space Administration (NASA).

CMIP6 models provide the state-of-the-art global climate model outputs that form the basis for several global initiatives, including the IPCC's scientific assessment of the climate status. For this work, 8 coupled models were selected and used for the historical period. Guided by data availability at the CEDA archive, uniform physics and initializations were selected across the models (p1 and i1 respectively), while three forcings (f1, f2 and f3) and two realizations (r1 and r10) were considered (Table 2). f1 includes prescribed time varying aerosol and ozone fields while f3 is characterized by interactive aerosol-cloud processes (Smith et al., 2020). The historical simulations are largely forced by observations including volcanic activity, solar variability and anthropogenic forcing (Eyring et al., 2016).

2.2 Methods

Comparative analysis of the annual cycle of the balance between rainfall and evapotranspiration, soil moisture and leaf area index were applied to investigate the response of soil water content and vegetation characteristics to the availability or deficit of rainfall. The characterization of annual cycles is also useful to gauge the representation of the seasonality of native land-atmosphere processes in the models. The effective rainfall, which is represented as the moisture convergence in the atmosphere, was defined as the difference between the total rainfall and the evapotranspiration (P-E) as used by Byrne et al (2015).

Figure 1 shows the regions of focus for this study. Dense vegetation exists in Central Africa (CA) and parts of West Africa (WA). Regions in the Horn of Africa, largely parts of Kenya (KE) and Somalia (SO), the Sahel (SH) and Southern Africa (SA) have much lower density of vegetation. The Sahara has the least vegetation over Africa. LAI, which is a crucial parameter in climate models, plays an important role in controlling the fluxes of energy, moisture and carbon (Richardson et al., 2020).

The condition of vegetation is sometimes used as a proxy for soil moisture at the root zone (Anderson et al. 2012). Wet regimes are likely in equatorial Africa and some coastal regions; the Sahara is a dry regime with too little moisture to influence turbulent fluxes at the surface. The key forcings of vegetation; net radiation in humid zones, precipitation in arid and semi-arid climates and temperature in extra-tropics (Nemani et al., 2003) are also useful in the characterizations of soil moisture regimes.

The terrestrial coupling index (TCI) was computed as the product of the standard deviation of soil moisture, and the correlation coefficient between soil moisture and latent heat flux as defined by Dirmeyer, (2011). This is necessary to account for the variability of soil moisture as the forcing variable. In regions with little variability, such as deserts or persistently saturated soils, the TCI is at a minimum as soil moisture is not a factor in the variability of latent heat flux (Halder et al., (2018)). The atmospheric leg of the coupling process, given by the atmospheric coupling index (ACI) was computed in a similar manner with the TCI, whereas temperature is the response variable to forcing by latent heat.

The uppermost soil layer was considered for all the datasets. This corresponds to 7 cm for ERA5, 5 cm for HadGEM3-G31-LL and 10 cm for the rest of the models. This is based on model results by Zhang et al (2011) who noted that soil moisture in the uppermost layer (10 cm) is a dominant forcing for surface fluxes. Utilizing CMIP5, Dirmeyer et al., (2013) also noted that this depth was readily available and hence useful for studies on the intercomparsion between models. The surface layer is affected through direct evaporation while the root zone depth drives the transpiration in the vegetation (Anderson et al., 2012). Vegetation indicators, such as NDVI or LAI, may also be used as a proxy to the soil moisture in the root zone. For consistency with ERA5, conversion of model soil moisture from gravimetric to volumetric units was done (Xu et al., 2018);

$SM(m^3/m^3) = SM(kg/m2)\rho * H$ (1)

In Equation (1), ρ represents the density of water, 1000 kg/m^3 and H is depth of the soil layer in meters.

Underscoring the importance of both the soil moisture and evaporative fraction as drivers of the interactions between the land and the atmosphere, Seneviratne et al., (2010) and Koster et al., (2011) have used a soil moisture-evaporative fraction framework to characterize the interaction regimes as in Figure 2. For this analysis, latent heat flux (λE) was used in place of evaporative fraction (EF). Wet regimes are characterized by sufficient soil moisture, above the critical value, (θ_{CRIT}), but limited net radiation (R_n)while the dry features too little soil moisture, below the wilting point (θ_{WILT}), though with sufficient net radiation. Transitional zones between the dry and wet regimes may change the relationship between soil moisture and radiation amounts, depending on the prevailing season.

3. Results And Discussion

The results are presented and discussed in two parts: The annual cycle of key land-atmosphere parameters, and regimes of soil moisture, and spatial analysis of the indices of coupling between the land and the atmosphere during MAM.

3.1. Annual Cycles of Various Parameters

The annual cycles of P-E, SM and LAI were analyzed to assess the mean representation of these parameters over the key regions identified. In Central Africa (CA), which has two main rainfall seasons, P-E has the main peak in November and a secondary one in March, which coincides with SM (Figure 3). On the other hand, LAI has the main peak in April. Though CMIP6 models differ substantially in magnitudes during the peak P-E seasons, they do broadly capture the bimodal cycle in ERA5. Models in CMIP5 differ in simulating the seasonality and magnitudes of precipitation over Central Africa, though a general wet bias is maintained (Aloysius et al., 2016). Figure 3 shows that there is a consistent under-estimation of SM throughout the year except in the HadGEM3-GC31-LL model, which has a substantial overestimate. This may be related with LAI under-estimation in the models with the exception of UKESM1-0-LL and CanESM5. In this region, both SM and LAI peak together with rainfall, in both reference datasets and

models. This is with the exception of CanESM5, which, despite having exceptionally high rainfall, depicts an unusual decline in the LAI between June and November.

Southern Africa has a unimodal pattern of P-E, peaking in January (Figure 3). With the exception of CanESM5 and MIROC6, most models indicate that the region experiences sustained moisture deficit throughout the year. In part, this is a weakness of the spatial averaging that includes the Namib desert. There are more pronounced magnitudes of divergence between the models during the DJF season as compared to the rest of the year. In this region, most models tend to overestimate SM, with the exception of GISS-E2-1-G and CanESM5, with the latter having a positive P-E. Similar to the CA, GISS-E2-1-G and UKESM1-0-LL stand out as models that, on average, have the least and highest LAI, respectively. Based on P-E, we note that models tend to show similarity during the dry seasons, and divergence during the peak rainfall season for both SM and LAI. This may hint that the representation of SM and LAI in the models is sensitive to rainfall biases.

Over East Africa, P-E is largely bimodal over both KE and SO (Figure 4), with the net moisture deficit dominating the Horn of Africa, while the rainfall seasons of OND and MAM, have excess rainfall in KE. Despite differences in the minor peak of P-E in November, the models have agreement that the peak of SM coincides with that of rainfall during the short rains season. CNRM-CM6-1, GISS-E2-1-G and HadGEM3-GC31-LL simulate the first peak of rainfall a month earlier, in October, while all models, though with a negative bias, consistently capture the time of the peak in April. MIROC6 is exceptionally wet with a late OND onset in November and an early onset in MAM and does not show a dry season between December and March. Consequently, soil moisture remains at peak levels from December to April. P-E peaks in October for CNRM-CM6-1, GISS-E2-1-G, HadGEM3-GC31-LL, and in December for MIROC6, while UKESM1-0-LL, with minimum bias, together with MRI-ESM2-0 and GFDL-CM4 place the peak rightly in November. Unlike observations, models have more rainfall during the short rains over the long rains season, with remarkable wet and dry biases respectively. Despite the differences in P-E, SM peaks in October-November and April for all models, except for HadGEM3-GC31-LL; peaks of LAI lag by a month.

In SO, P-E peaks in October, but it is largely overestimated by the models. P-E also peaks in April, but the corresponding seasonality of soil moisture is largely variable across the models. CanESM5 and GISS-E2-1-G have nearly invariant LAI at minimum, while at maximum, UKESM1-0-LL shows invariant seasonality. The rest of the models tend to oscillate in magnitude within the GIMMS annual range. SM peaks coincidentally with P-E while LAI lags behind by one month.

Results for West Africa and the Sahel in Figure 5 indicate that the seasonality is unimodal, with fair model agreement during the dry seasons and a large spread during the P-E peak during the West African monsoon season. In most models, vegetation peaks a month after the P-E and SM maxima. Models such as GISS-E2-1-G and UKESM-1-0-LL that underestimate P-E during the peak season, also underestimate SM throughout the year. HadGEM3-GC31-LL overestimates the soil moisture during the rainfall season in WA and underestimates it in the SH. On the other hand, vegetation peaks in October, with variable

patterns of the seasonality across models. GISS-E2-1-G has the least vegetation while CanESM5 has the highest amount.

Utilizing CMIP5-ESMs, Mahowald et al., (2016) reported that some models do not clearly show the precipitation-vegetation response. This is despite the expectation that the LAI in the tropics is controlled by availability of moisture, unlike in the higher latitudes where the control of moisture by temperature is dominant (Zeng et al., 2013). Lack of such a relationship may point to a weakness in the model configurations, which may cause inaccurate representation of the boundary layer processes as well as the cycles of surface water, energy and carbon (Park and Jeong, 2021). This is likely to be true for GISS-E2-1-G and CanESM5 that show nearly invariant and low LAI in all regions over Africa, while UKESM1-0-LL overestimates this parameter. CanESM5 has erroneously decreasing LAI over Central Africa in June to October, with minimum and nearly invariant values over East Africa and the Sahel. Considering that the response of vegetation to climatic forcing is region-specific, it is important to be cautious in generalizing these results over Africa where we have a variety of vegetation cover (Wu et al., 2015). Given that vegetation plays a critical control in the process of evapotranspiration, inaccurate representation of LAI could introduce uncertainties in the cycles of both energy and water and potentially affect the characteristics of coupling between the land and the atmosphere (Williams and Torn, 2015).

3.2. Soil Moisture Regimes

In order to characterize the soil moisture regimes in regions highlighted in, soil moisture-latent heat scatter plots with Locally Weighted Scatterplot Smoothing (LOWESS) curves based on ERA5 are presented in Figure 6 for the months of March to May over the 1979-2014 period. In regions where SM can reach high levels, such as CA (>0.37 m^3/m^3) the response of HFLS to SM levels out, indicating transition into a wet regime. In the Sahel, given that March-May is a dry season, most soil moisture records fall below 0.06 m^3/m^3 and with minimal indication of latent heat response, which is indicative of a dry regime. Direct linear relationships between soil moisture and latent heat flux exist over East Africa (KE & SO), West Africa (WA) and to some degree, over SA (at lower SM levels). This indicates that during the March-May season, soil moisture is an important forcing to the fluxes at the lower boundary over the regions in the eastern, southern and western parts of Africa. The SH is too dry while the relationship only holds for lower SM levels in the CA.

SM forcing to the boundary layer fluxes exists in transition zones that fall in between dry and wet regimes (Figure 2). This is true for KE, SO, WA and partly SA (Figure 6). This analysis shows the potential for L-A coupling at different regions in Africa, depending on the seasonality of soil moisture. In dry soils, there is negligible SM forcing to HFLS while in saturated soils, HFLS is controlled by net radiation, which in turn depletes SM.

We investigate how models represent the regimes of soil moisture and latent heat flux for two case areas; a wet regime over Central Africa (CA) and a transitional zone over East Africa (KE). The results are presented in Figures 7 and 8 respectively. Over CA, MRI-ESM2-0 closely simulates the ERA5 patterns of

soil moisture and latent heat flux. CNRM-CM6-1, GISS-E2-1G, HadGEM3-GC31-LL and UKESM1-0-LL though able to simulate the pattern of SM at low levels, do not correctly capture the pattern of HLFS at peak SM as in ERA5. In MIROC6 and CanESM5, the relationship is at minimum, with correlation scores of 0.17 and 0.29. On the other hand, GFDL-CM4 simulates an inverse relationship with a correlation score of -0.54, implying that HFLS depletes SM. The annual cycle results in Figure 3 indicated that MIROC6, CanESM5 and GFLD-CM4 similarly portrayed the highest positive P-E bias for most parts of the year.

Over KE, the models are able to simulate the soil moisture-latent heat relationship with correlations above 0.9 despite the biases in the magnitudes of the parameters under consideration, which is an indication that the patterns of land-atmosphere feedbacks over East Africa are well simulated in the models.

3.2. Land-Atmosphere Coupling Indices

Terrestrial and atmospheric coupling indices based on ERA5 are presented in Figure 9. Regions of strong positive TCI (shown in brown) indicate robust coupling between SM and HFLS, while negative values (in green) indicate that surface fluxes increase at the expense of soil moisture, hence no coupling exists in these regions. The hatching indicates significant correlations at 95% confidence interval. Regions south of the Sahel, in East Africa and Southern Africa have strong soil moisture-latent heat coupling. In these regions, soil moisture forcing is a key driver for latent heat variability during the MAM season. The Sahara, though with significant correlations, does not have significant coupling as the variability of soil moisture is minimal being in a dry regime (Figure 6 and Supplementary plots, Figure S2). Central Africa, despite having the highest amounts of soil moisture, does not show a significant forcing of soil moisture on latent heat flux. It is only in this region where the correlations are not significant or are significant with negative sign. Given the seasonal and vegetation characteristics, evapotranspiration, driven by net radiation, is the major driver of surface fluxes over Central Africa. Given that MAM is an active rainfall season in equatorial Africa, the influence of soil moisture on lower boundary fluxes, especially over the eastern side, may contribute to the overall seasonal characteristics.

The ACI indicates that latent heat control of 2metre temperature exists over parts of East Africa, Southern Africa and south of the Sahel. The Sahara and Central Africa are regions where lower boundary temperature is not controlled by latent heat variability. These we also previously identified as dry and wet regimes respectively, Figure 6.

In general, L-A coupling exists where both the terrestrial and atmospheric pathways co-exist. This is true for East Africa and the regions south of the Sahel. In southern Africa, the region of strong ACI is shifted northward compared to TCI, indicating that the local coupling is sensitive to the northward shift of the rainfall which is a key forcing generating soil moisture anomalies. Interestingly, negative TCI and a positive ACI over Central Africa indicates that latent heat fluxes are associated with depleted soil moisture, and hence no coupling for both terrestrial and atmospheric pathways. Where coupling exists, positive anomalies of soil moisture would trigger anomalous increases in latent heat, which in turn raise the evaporative fraction, resulting in a negative anomaly of near surface temperature. The coupling patterns are sensitive to the prevailing climate conditions; in off-season regions in the Sahel, the soils are

dry during this season, while in the southern Africa, presence of land-atmosphere coupling signal is indicative of soil moisture memory from the preceding months (Dirmeyer at al., 2009). Over East Africa, the existence of land-atmosphere coupling has been linked with the increase in surface temperatures during extended drought seasons when anomalously low soil moisture levels are recorded (Abera et al., 2018).

The coupling characteristics in ERA5 can be explained by the interannual the forcing variables; soil moisture and latent heat, shown in Figure 10. Indeed, significant forcing can only be exerted if the forcing variable is not constant and a degree of variability is triggered in the response variable. Given that correlations are significant in most regions over Africa, the inclusion of a measure of variability is therefore useful to overcome the weakness of simple linear relationships. The high variability of soil moisture and latent heat over East Africa, stretching to West Africa and parts of Southern Africa coincides with strong TCI and ACI, Figure 9. Isolated regions of peak variability accordingly correspond also to peaks in TCI or ACI. Less variability in the Sahara and in Central Africa is an indication of dry and wet regimes, respectively.

The results of TCI based on models are presented in Figure 11. GISS-E2-1-G and CNRM-CM6-1 have overall weakest TCI over Africa. The HadGEM3-G31-LL and UKESM1-0-LL MOHC models tend to overestimate the strength of TCI over most regions of Africa, including parts of Central Africa. The rest of the models, especially MIROC6, GFDL-CM4 and CanESM5, which could not properly simulate the soil moisture regimes over Central Africa (Figure 7), indicate an eastward and southern expansion to the region of lack of soil moisture-latent heat coupling (shown in green). Notably, MIROC6 indicates no coupling over the Ethiopian highlands. The south of the Sahel region, spreading from Ethiopia to West Africa, has much stronger TCI in HadGEM3-GC31-LL, UKESM1-0-LL and CanESM5. The coupling zone stands out in MIROC6 but is shifted northwards to about 15^{o} latitude compared to the ERA5 pattern, which does not go beyond 13^{o} latitude. Over Madagascar, there is no consensus between the models, although CNRM-CM6-1, MRI-ESM2-0 and GFDL-CM4 closely resemble the ERA5 data. In the East Africa region, models show good correspondence with ERA5, despite the tendency to overestimate the intensity with the exception of GFDL-CM4, CNRM-CM6-1 and GISS-E2-1-G.

Models with low and weak seasonality in LAI (Figures 3-5), such as CNRM-CM6-1 and GISS-E2-1-G, tend to have overall weaker TCI, without highlighting regions of strong coupling. This may be related to weakness in capturing evapotranspiration that has control on latent heat flux (Williams and Torn, 2015).

In Figure 12, ACI in models is presented. CNRM-CM6-1 stands out with strongest ACI over Southern, East and erroneously over eastern Central Africa, despite the model showing weak TCI all over Africa. This may be attributed to the high interannual variability in these regions (Supplementary plots, Figure S3) and a more pronounced negative bias in HFLS (Supplementary plots, Figure S5). The nature of the bias and variability may result in a weak response of the latent heat to the soil moisture, but an amplified signal in forcing to temperature. However, this pattern is not consistent through the models. This is an indication that the relationships are model specific, and the variability or biases of similar magnitudes do not

generate comparable responses between models (Koster et al., 2009, Berg et al., 2009). Similar to the TCI, GISS-E2-1-G portrayed the overall weakest ACI with the exception of limited regions bordering Tanzania, Mozambique, Malawi and Zambia. However, these are not regions of coupling between latent heat and temperature based on ERA5. Although the mean biases of latent heat are not high, it shows that the variability of the variables are not strongly linked as both terrestrial and atmospheric pathways are weaker than in ERA5. The models presented generally show consensus on strong coupling over southern Africa, with exception of the eastern regions bordering Lesotho. Though with a tendency to extend the coupling southwards, models generally represent the coupling between latent heat and temperature in Southern Africa.

Over East Africa, MOHC models and GISS-E2-1G have the weakest ACI, with the rest of the models indicating signals of coupling between latent heat and temperature over southern Africa in agreement with ERA5. This coupling spans from the east of Lake Victoria towards the Horn of Africa extending northward while excluding the Ethiopian highlands. Similar to ERA5, a weaker coupling zone exists in the South Sudan-Chad-Central Africa Republic region extending westwards for CNRM-CM6-1 and GFDL-CM4.

Therefore, there is model agreement on the atmospheric pathway over Southern Africa, but differences exist over East Africa. Despite these differences, most models agree on the lack of coupling in the Sahara and Central Africa. This points to a realistic behavior of the models at the extremes of the SM spectrum. Largely, most models overestimate the terrestrial coupling leg over southern and eastern Africa. Previous results by Lei et al., (2018) and Dirmeyer et al., (2018) show consensus that most global models are biased to overestimate the strength of the coupling. Although both TCI and ACI are co-located in ERA5, this is not true over East Africa for GISS-E2-1-G, HadGEM3-GC31-LL and UKESM1-0-LL. This indicates that latent heat is not an important control of temperature in these models over East Africa. Given that MAM is the main rainfall season for East Africa, it may be hypothesized that the control of temperature is related to net radiation (cloud cover), rather than surface fluxes in these models.

GISS-E2-1-G has minimum variability of both the soil moisture and latent heat, and consequently, the strength of the coupling indices is damped. The strong variability in HadGEM3-GC31-LL soil moisture may be attributed to the consideration of a much shallower depth of 5cm. This results in a strong TCI. Despite strong variability of latent heat, temperature coupling is only strong over Southern Africa, where both variables tend to have significant variability. It is only in these areas, and some parts of East and West Africa, where the correlations are significant. Models tend to agree on high variability of temperature, soil moisture and latent heat flux over Southern Africa, (Supplementary plots, Figure S3 & S4), hence consensus on the coupling indices over this region. These results indicate that the mean biases are not necessarily determinants of the coupling patterns. Rather, the internal variability of the models determines the nature of the coupling. This makes the results specific to the models based on their varied parameterizations (Lei et al., 2018). Models that over-estimate the land-atmosphere coupling tend also to erroneously amplify temperature extremes, (Ukkola et al., 2018). GLACE-CMIP5 results by Zhou et al (2019) indicates that soil moisture coupling amplifies drought events in historical and future timescales. Historical observations have also confirmed that prolonged droughts are usually located in

regions of strong LA coupling (Cook et al., 2010 and Miralles et al., 2014). Miralles et al., (2014) noted that even with pre-existing synoptic conditions, negative anomalies of soil moisture played a role in the intensification of the major heatwave events of 2003 and 2010 in Europe. It is therefore paramount that models accurately represent the land-atmosphere interactions in order to provide reliable information on the current and future climate hazards.

4. Summary And Conclusion

We have evaluated the coupling between the land and atmosphere in selected CMIP6 models over diverse climatic zones in Africa ranging from humid zones in the Congo to deserts in the Sahara. The seasonality in P-E, SM and LAI is well represented, despite biases in magnitudes. Unique biases were however noted over East Africa, where P-E was more OND than MAM. With exception of UKESM1-0-LL and CasESM5, underestimation of LAI in the rest of the models could be attributed to dry SM and P-E biases. Models tend to overestimate the precipitation-evapotranspiration balance in the peak rainfall months over Africa except the long rains over East Africa (KE) that have a dry bias. Models accurately represented the soil moisture limited regime over East Africa, while for over the wet regime in Central Africa, half of the models surveyed could not simulate the soil moisture-latent heat flux regime. This indicates that interactive processes such as the coupling between the soil moisture and latent heat as represented in models is sensitive to the local climate. This may be controlled by the specified land surface and boundary layer parameterizations.

Despite consideration of a shallower soil moisture depth in the HadGEM3-GC3-1-LL, soil moisture levels were surprisingly lower compared to other models and ERA5 datasets, especially during the peak season in the SH and SO regions. Although no outright deductions can be made, this underscores the findings of Santanello et al. (2011a) that in dry regimes, the performance of the land surface models outweighs the boundary layer parameterizations, unlike in the wet regimes. It is therefore important to ensure that land surface parameters are accurately represented in models, especially in semi-arid zones that are also hot spots for land-atmosphere interactions.

ERA5 data indicated that regions in West Africa to East Africa, and parts of Southern Africa, are regions of strong coupling during the March-May season. Most of the models overestimate the strength of the coupling in these regions. Inter-model differences are related to the model inter-annual variability, rather than the mean biases. For instance, GISS-E2-1-G had overall least inter-annual variability of both soil moisture and latent heat, resulting in the least strength of both TCI and ACI. On the other hand, HadGEM3-GC31-LL's strong TCI over East and southern Africa is related to the highest standard deviation of soil moisture over those regions. In regions of strong coupling, soil moisture is an important forcing of the local/regional climate.

The evaluation of land-atmosphere interactions in this study can inform the development of robust land surface packages in the next generation climate models beyond CMIP6. This study noted that focus on improvement of the inter-annual variability of models, together with biases, are key aspects that can

enhance the overall performance of climate models, especially on land surface forcing to the atmosphere.

Declarations

Conflicts of interest/Competing interests

No conflict of interest

Data availability

The datasets generated during and/or analysed during the current study are available from the corresponding author on reasonable request

Code availability

Some codes used for the analysis can be found on Github https://github.com/Priority-on-African-Diagnostics/UoN

Acknowledgements

CMIP6 model outputs used in this study were accessed from the CEDA archive in the JASMIN super-data cluster. ERA5 reanalysis was sourced from the CDS while the GIMMS-LAI3g version 2 was available from NASA's ORNL DAAC portal. This research was supported by the LaunchPAD research fellowship, as part of the Future Climate for Africa (FCFA) programme.

References

1. Abera TA, Heiskanen J, Maeda EE, Pellikka PK (2020) Land surface temperature trend and its drivers in East Africa.*Journal of Geophysical Research: Atmospheres*, *125*(23), e2020JD033446.
2. Aloysius NR, Sheffield J, Saiers JE, Li H, Wood EF (2016) Evaluation of historical and future simulations of precipitation and temperature in central Africa from CMIP5 climate models. Journal of Geophysical Research: Atmospheres 121(1):130–152
3. Anderson WB, Zaitchik BF, Hain CR, Anderson MC, Yilmaz MT, Mecikalski J, Schultz L (2012) Towards an integrated soil moisture drought monitor for East Africa. Hydrol Earth Syst Sci 16(8):2893–2913
4. Bader J (2003),), *and* M. Latif *(* The impact of decadal-scale Indian Ocean sea surface temperature anomalies on Sahelian rainfall and the North Atlantic oscillation, Geophys. Res. Lett., 30*(*22*)*, 2169, *doi:10.1029/2003GL018426.*
5. Behera SK, Yamagata T (2001) Subtropical SST dipole events in the southern Indian Ocean. Geophys Res Lett 28:327–330

6. Berg A, Findell K, Lintner B, Giannini A, Seneviratne SI, Van Den Hurk B, Lorenz R, Pitman A, Hagemann S, Meier A, Cheruy F (2016) Land–atmosphere feedbacks amplify aridity increase over land under global warming. Nature Climate Change 6(9):869–874
7. Betts AK, Silva Dias MAF (2010) Progress in understanding land-surface-atmosphere coupling from LBA research.*Journal of Advances in Modeling Earth Systems*, *2*(2)
8. Byrne MP, O'Gorman PA (2015) The response of precipitation minus evapotranspiration to climate warming: Why the "wet-get-wetter, dry-get-drier" scaling does not hold over land. J Clim 28(20):8078–8092
9. Careto JAM, Cardoso RM, Soares PMM, Trigo RM (2018) Land-Atmosphere Coupling in CORDEX-Africa: Hindcast Regional Climate Simulations. Journal of Geophysical Research: Atmospheres 123(19):11–048
10. Chahine MT (1992) GEWEX: The global energy and water cycle experiment. Eos, Transactions American Geophysical Union 73(2):9–14
11. Chen T, Van Der Werf GR (2014) RaM De Jeu, Liu YY, Van Der Werf GR, Dolman AJ *()* Using satellite based soil moisture to quantify the water driven variability in NDVI: a case study over mainland Australia. *Remote Sensing of Environment, 140, 330–338.*
12. Cook BI, Bonan GB, Levis S (2006) Soil moisture feedbacks to precipitation in southern Africa. J Clim 19(17):4198–4206
13. Cook ER, Anchukaitis KJ, Buckley BM, D'Arrigo RD, Jacoby GC, Wright WE (2010) Asian monsoon failure and megadrought during the last millennium. Science 328(5977):486–489
14. Cook KH (1999) Generation of the African easterly jet and its role in determining West African precipitation. J Clim 12(5):1165–1184
15. Cook KH (1999) Generation of the African easterly jet and its role in determining West African precipitation. J Clim 12(5):1165–1184
16. Cook KH, Vizy EK (2016) The Congo Basin Walker circulation: dynamics and connections to precipitation. Clim Dyn 47:697–717. https://doi.org/10.1007/s00382-015-2864-y
17. Crowhurst D, Dadson S, Peng J, Washington R (2020) Contrasting controls on Congo Basin evaporation at the two rainfall peaks.*Climate Dynamics*,1–16
18. Dirmeyer PA, Jin Y, Singh B, Yan X (2013) Trends in land–atmosphere interactions from CMIP5 simulations. J Hydrometeorol 14(3):829–849
19. Dirmeyer PA (2011) A history and review of the Global Soil Wetness Project (GSWP). J Hydrometeorol 12(5):729–749
20. Dyer EL, Jones DB, Li R, Sawaoka H, Mudryk L (2017) Sahel precipitation and regional teleconnections with the Indian Ocean. Journal of Geophysical Research: Atmospheres 122(11):5654–5676
21. Eyring V, Bony S, Meehl GA, Senior CA, Stevens B, Stouffer RJ, Taylor KE (2016) Overview of the Coupled Model Intercomparison Project Phase 6 (CMIP6) experimental design and organization.

Geosci Model Dev 9(5):1937–1958

22. Findell KL, Berg A, Gentine P, Krasting JP, Lintner BR, Malyshev S, Shevliakova E (2017) The impact of anthropogenic land use and land cover change on regional climate extremes. Nat Commun 8(1):1–10
23. Gelaro R, McCarty W, Suárez MJ, Todling R, Molod A, Takacs L, Zhao B (2017) The modern-era retrospective analysis for research and applications, version 2 (MERRA-2). J Clim 30(14):5419–5454
24. Hagos SM, *and* K. H. Cook *(*2008*)*, Ocean warming and late-twentieth-century Sahel drought and recovery,J. Clim., 21*(*15*)*,3797–3814
25. Hersbach H, Bell B, Berrisford P, Hirahara S, Horányi A, Muñoz-Sabater J, Thépaut JN (2020) The ERA5 global reanalysis. Q J R Meteorol Soc 146(730):1999–2049
26. Hirsch AL, Pitman AJ, Seneviratne SI, Evans JP, Haverd V (2014) Summertime maximum and minimum temperature coupling asymmetry over Australia determined using WRF. Geophys Res Lett 41:1546–1552. doi:10.1002/2013GL059055
27. Hohenegger C (2020) Land–Atmosphere Interaction in Tropical Africa. In *Oxford Research Encyclopedia of Climate Science*
28. Hurk BVD, Kim H, Krinner G, Seneviratne SI, Derksen C, Oki T, Douville H, Colin J, Ducharne A, Cheruy F, Viovy N (2016) LS3MIP (v1. 0) contribution to CMIP6: the Land Surface, Snow and Soil moisture Model Intercomparison Project–aims, setup and expected outcome. Geosci Model Dev 9(8):2809–2832
29. Indeje M, Semazzi FH, Ogallo LJ (2000) ENSO signals in East African rainfall seasons. International Journal of Climatology: A Journal of the Royal Meteorological Society 20(1):19–46
30. Indeje M, Semazzi FH, Ogallo LJ (2000) ENSO signals in East African rainfall seasons. International Journal of Climatology: A Journal of the Royal Meteorological Society 20(1):19–46
31. Koster RD, Sud YC, Guo Z, Dirmeyer PA, Bonan G, Oleson KW, Xue Y (2006) GLACE: the global land–atmosphere coupling experiment. Part I: overview. J Hydrometeorol 7(4):590–610
32. Koster RD, Guo Z, Yang R, Dirmeyer PA, Mitchell K, Puma MJ (2009) On the nature of soil moisture in land surface models. J Clim 22(16):4322–4335
33. Koster RD, Mahanama SPP, Yamada TJ, Balsamo G, Berg AA, Boisserie M, Dirmeyer PA, Doblas-Reyes FJ, Drewitt G, Gordon CT, Guo Z (2011) The second phase of the Global Land–Atmosphere Coupling Experiment: Soil moisture contributions to subseasonal forecast skill. J Hydrometeorol 12(5):805–822
34. Koster RD, Sud YC, Guo Z, Dirmeyer PA, Bonan G, Oleson KW, Chan E, Verseghy D, Cox P, Davies H, Kowalczyk E (2006) GLACE: the global land–atmosphere coupling experiment. Part I: overview. J Hydrometeorol 7(4):590–610
35. Lee JY, Marotzke J, Bala G, Cao L, Corti S, Dunne JP, Engelbrecht F, Fischer E, Fyfe JC, Jones C, Maycock A, Mutemi J, Ndiaye O, Panickal S, Zhou T (2021) Future Global Climate: Scenario- Based Projections and Near-Term Information. In: *Climate Change 2021: The Physical Science Basis. Contribution of Working Group I to the Sixth Assessment Report of the Intergovernmental Panel on*

Climate Change [Masson-Delmotte, V., P. Zhai, A. Pirani, S. L. Connors, C. Péan, S. Berger, N. Caud, Y. Chen, L. Goldfarb, M. I. Gomis, M. Huang, K. Leitzell, E. Lonnoy, J. B. R. Matthews, T. K. Maycock, T. Waterfield, O. Yelekçi, R. Yu and B. Zhou (eds.)]. Cambridge University Press. In Press

36. Lei F, Crow WT, Holmes TR, Hain C, Anderson MC (2018) Global investigation of soil moisture and latent heat flux coupling strength. Water Resour Res 54(10):8196–8215
37. Liang X, Guo J (2003) Intercomparison of land-surface parameterization schemes: sensitivity of surface energy and water fluxes to model parameters. J Hydrol 279(1–4):182–209
38. Lorenz R, Argüeso D, Donat MG, Pitman AJ, van den Hurk B, Berg A, Lawrence DM, Chéruy F, Ducharne A, Hagemann S, Meier A (2016) Influence of land-atmosphere feedbacks on temperature and precipitation extremes in the GLACE-CMIP5 ensemble. Journal of Geophysical Research: Atmospheres 121(2):607–623
39. Mahowald N, Lo F, Zheng Y, Harrison L, Funk C, Lombardozzi D, Goodale C (2016) Projections of leaf area index in earth system models. Earth Sys Dyn 7(1):211–229
40. Marchant R, Mumbi C, Behera S, Yamagata T (2007) The Indian Ocean dipole–the unsung driver of climatic variability in East Africa. Afr J Ecol 45(1):4–16
41. Merchant CJ, Paul F, Popp T, Ablain M, Bontemps S, Defourny P, Hollmann R, Lavergne T, Laeng A, De Leeuw G, Mittaz J (2017) Uncertainty information in climate data records from Earth observation. Earth System Science Data 9(2):511–527
42. Miralles DG, Teuling AJ, Van Heerwaarden CC, De Arellano JVG (2014) Mega-heatwave temperatures due to combined soil desiccation and atmospheric heat accumulation. Nat Geosci 7(5):345–349
43. Miralles DG, Teuling AJ, Van Heerwaarden CC, De Arellano JVG (2014) Mega-heatwave temperatures due to combined soil desiccation and atmospheric heat accumulation. Nat Geosci 7(5):345–349
44. Miralles DG, Van Den Berg MJ, Teuling AJ, De Jeu RAM (2012) Soil moisture-temperature coupling: A multiscale observational analysis.*Geophysical Research Letters*, *39*(21)
45. Nicholson S (2000) Land surface processes and Sahel climate. Rev Geophys 38(1):117–139
46. Nicholson SE (2000) The nature of rainfall variability over Africa on time scales of decades to millenia. Glob Planet Change 26(1–3):137–158
47. Nogherotto R, Coppola E, Giorgi F, Mariotti L (2013) Impact of Congo Basin deforestation on the African monsoon. Atmospheric Science Letters 14(1):45–51
48. Ogallo LJ, JE J (1988) Teleconnection between seasonal rainfall over East Africa and global sea surface temperature anomalies. Journal of the Meteorological Society of Japan Ser II 66(6):807–822
49. Omeny PA, Ogallo LABAN, Okoola R, Hendon HARRY, and MATHEW WHEELER (2006). "East African rainfall variability associated with the Madden-Julian Oscillation."*Journal of Kenya Meteorological SocietyVolume* 2, no. 2
50. Park H, Jeong S (2021) Leaf area index in Earth system models: how the key variable of vegetation seasonality works in climate projections. Environmental Research Letters 16(3):034027

51. Park S, Kang D, Yoo C, Im J, Lee MI (2020) Recent ENSO influence on East African drought during rainy seasons through the synergistic use of satellite and reanalysis data. ISPRS Journal of Photogrammetry and Remote Sensing 162:17–26
52. Peng J, Dadson S, Leng G, Duan Z, Jagdhuber T, Guo W, Ludwig R (2019) The impact of the Madden-Julian Oscillation on hydrological extremes. J Hydrol 571:142–149
53. Pokam WM, Bain CL, Chadwick RS, Graham R, Sonwa DJ, Kamga FM (2014) Identification of processes driving low-level westerlies in west equatorial Africa. J Clim 27(11):4245–4262
54. Pyke CR, Andelman SJ (2007) Land use and land cover tools for climate adaptation. Clim Change 80(3):239–251
55. Quesada B, Arneth A, Robertson E, de Noblet-Ducoudré N (2018) Potential strong contribution of future anthropogenic land-use and land-cover change to the terrestrial carbon cycle. Environmental Research Letters 13(6):064023
56. Reason CJC, Jagadheesha D (2005) A model investigation of recent ENSO impacts over southern Africa. Meteorol Atmos Phys 89(1):181–205
57. Saji NH, Goswami BN, Vinayachandran PN, Yamagata T (1999) A dipole mode in the tropical Indian Ocean. Nature 401(6751):360–363
58. Santanello Jr JA, Dirmeyer PA, Ferguson CR, Findell KL, Tawfik AB, Berg A, Roundy J (2018) Land–atmosphere interactions: The LoCo perspective. Bull Am Meteorol Soc 99(6):1253–1272
59. Santanello Jr JA, Dirmeyer PA, Ferguson CR, Findell KL, Tawfik AB, Berg A, Ek M, Gentine P, Guillod BP, Van Heerwaarden C, Roundy J (2018) Land–atmosphere interactions: The LoCo perspective. Bull Am Meteorol Soc 99(6):1253–1272
60. Sherwood S, Fu Q (2014) A drier future? Science 343(6172):737–739
61. Smith CJ, Kramer RJ, Myhre G, Alterskjær K, Collins W, Sima A, Boucher O, Dufresne JL, Nabat P, Michou M, Yukimoto S (2020) Effective radiative forcing and adjustments in CMIP6 models. Atmos Chem Phys 20(16):9591–9618
62. Soares PM, Careto JA, Cardoso RM, Goergen K, Trigo RM (2019) Land-atmosphere coupling regimes in a future climate in Africa: From model evaluation to projections based on CORDEX-Africa. Journal of Geophysical Research: Atmospheres 124(21):11118–11142
63. Soares PM, Careto JA, Cardoso RM, Goergen K, Trigo RM (2019) Land-atmosphere coupling regimes in a future climate in Africa: From model evaluation to projections based on CORDEX-Africa. Journal of Geophysical Research: Atmospheres 124(21):11118–11142
64. Taylor K, Juckes M, Balaji V, Cinquini L, Denvil S, Durack P, Elkington M, Guilyardi E, Kharin S, Lautenschlager M, Lawrence B (2017) CMIP6 Global Attributes, DRS, Filenames, Directory Structure, and CVs.
65. Ukkola AM, Pitman AJ, Donat MG, De Kauwe MG, Angélil O (2018) Evaluating the contribution of land-atmosphere coupling to heat extremes in CMIP5 models. Geophys Res Lett 45(17):9003–9012

66. Williams IN, Torn MS (2015) Vegetation controls on surface heat flux partitioning, and land-atmosphere coupling. Geophys Res Lett 42(21):9416–9424
67. Wu D, Zhao X, Liang S, Zhou T, Huang K, Tang B, Zhao W (2015) Time-lag effects of global vegetation responses to climate change. Glob Change Biol 21(9):3520–3531
68. Wulfmeyer V, Turner DD, Baker B, Banta R, Behrendt A, Bonin T, Brewer WA, Buban M, Choukulkar A, Dumas E, Hardesty RM (2018) A new research approach for observing and characterizing land–atmosphere feedback. Bull Am Meteorol Soc 99(8):1639–1667
69. Xu Y, Wang L, Ross KW, Liu C, Berry K (2018) Standardized soil moisture index for drought monitoring based on soil moisture active passive observations and 36 years of north American land data assimilation system data: A case study in the southeast United States. *Remote Sensing*, *10*(2), p.301
70. Zeng FW, Collatz GJ, Pinzon JE, Ivanoff A (2013) Evaluating and quantifying the climate-driven interannual variability in Global Inventory Modeling and Mapping Studies (GIMMS) Normalized Difference Vegetation Index (NDVI3g) at global scales. Remote Sensing 5(8):3918–3950
71. Zheng Y, Kumar A, Niyogi D (2015) Impacts of land–atmosphere coupling on regional rainfall and convection. Clim Dyn 44(9–10):2383–2409
72. Zhou S, Williams AP, Berg AM, Cook BI, Zhang Y, Hagemann S, Lorenz R, Seneviratne SI, Gentine P (2019) Land–atmosphere feedbacks exacerbate concurrent soil drought and atmospheric aridity. *Proceedings of the National Academy of Sciences*, *116*(38), pp.18848-18853
73. Zhu Z, Bi J, Pan Y, Ganguly S, Anav A, Xu L, Samanta A, Piao S, Nemani RR, Myneni RB (2013) Global data sets of vegetation leaf area index (LAI) 3g and fraction of photosynthetically active radiation (FPAR) 3g derived from global inventory modeling and mapping studies (GIMMS) normalized difference vegetation index (NDVI3g) for the period 1981 to 2011. Remote sensing 5(2):927–948

Tables

Table 1 Overview of the Eight selected CMIP6 models analyzed in this study

Centre	Model	Variant ID	Spatial resolution (degrees)
CNRM-CERFACS	CNRM-CM6-1	r10i1p1f2	1.4 by 1.4
MOHC	UKESM1-0-LL	r1i1p1f2	1.25 by 1.875
MOHC	HadGEM3-G31-LL	r1i1p1f3	1.25 by 1.875
MRI	MRI-ESM2-0	r1i1p1f1	1.121 by 1.125
NASA	GISS-E2-1-G	r1i1p1f1	2 by 2.5
NOAA	GFDL-CM4	r1i1p1f1	1 by 1.25
MIROC	MIROC6	r10i1p1f1	1.4 by 1.4
CCCma	CanESM5	r10i1p1f1	2.791 by 2.8125

Figures

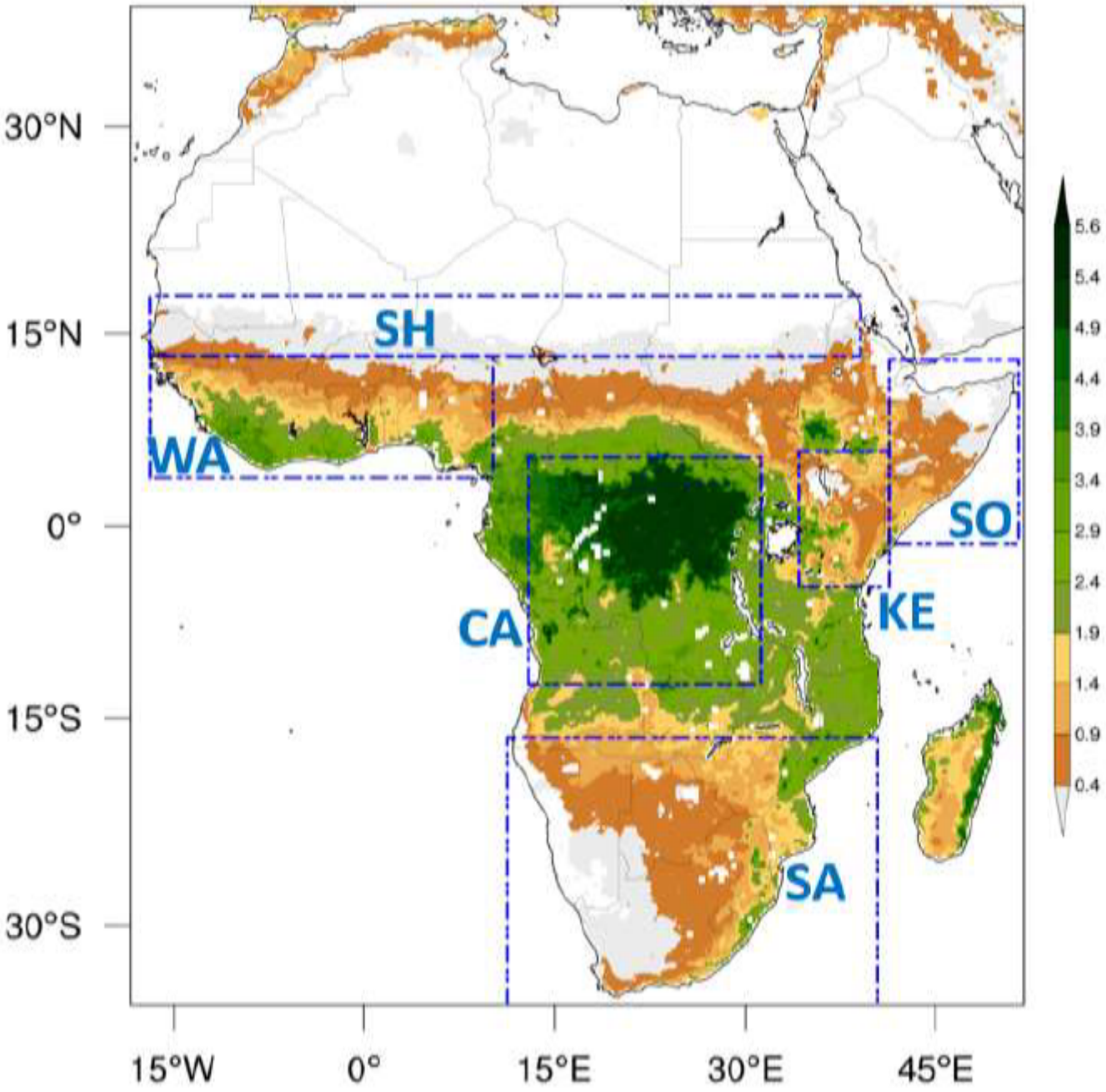

Figure 1

Mean leaf area index over Africa based on GIMMS-LAI3g version 2 for MAM season over the period 1981-2015

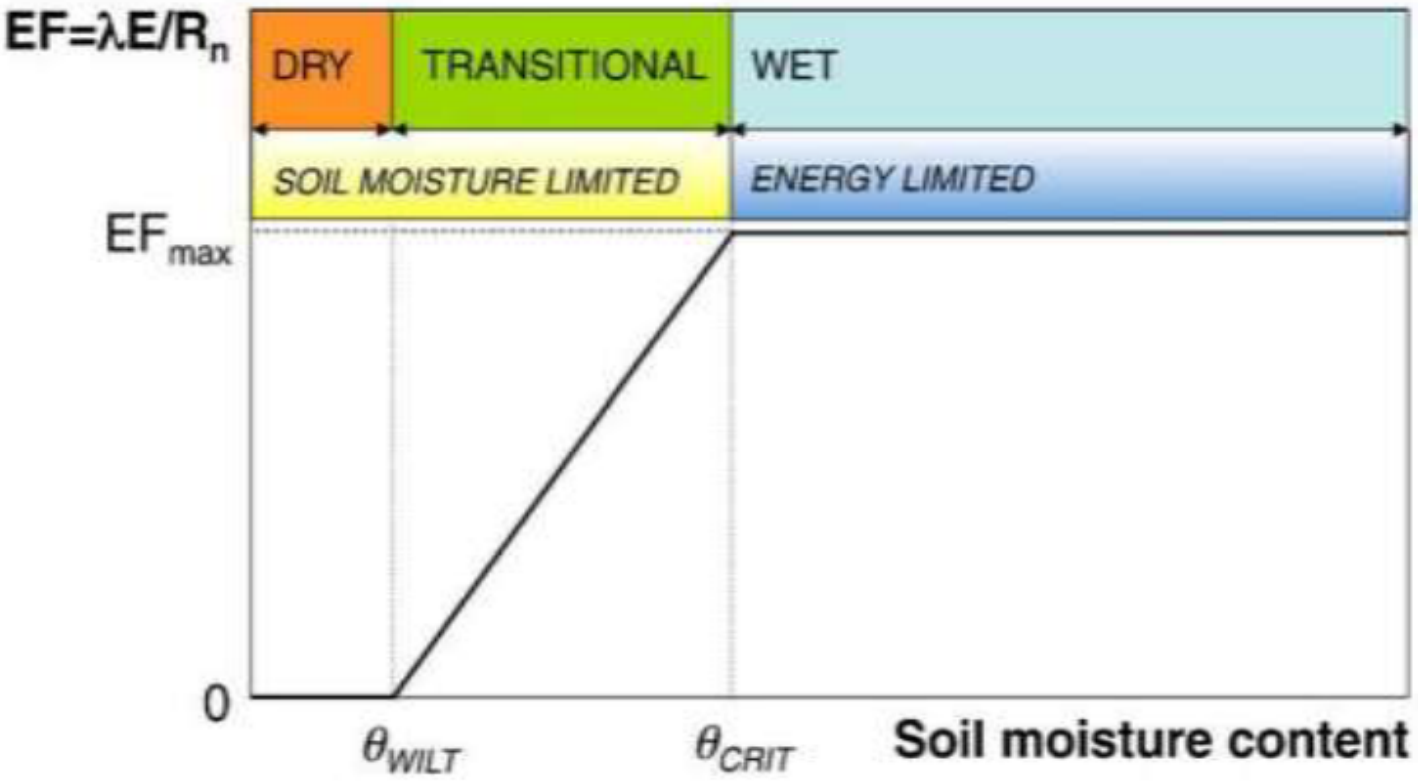

Figure 2

Characterization of soil moisture content and the evaporative fraction regimes (Seneviratne et al., 2010)

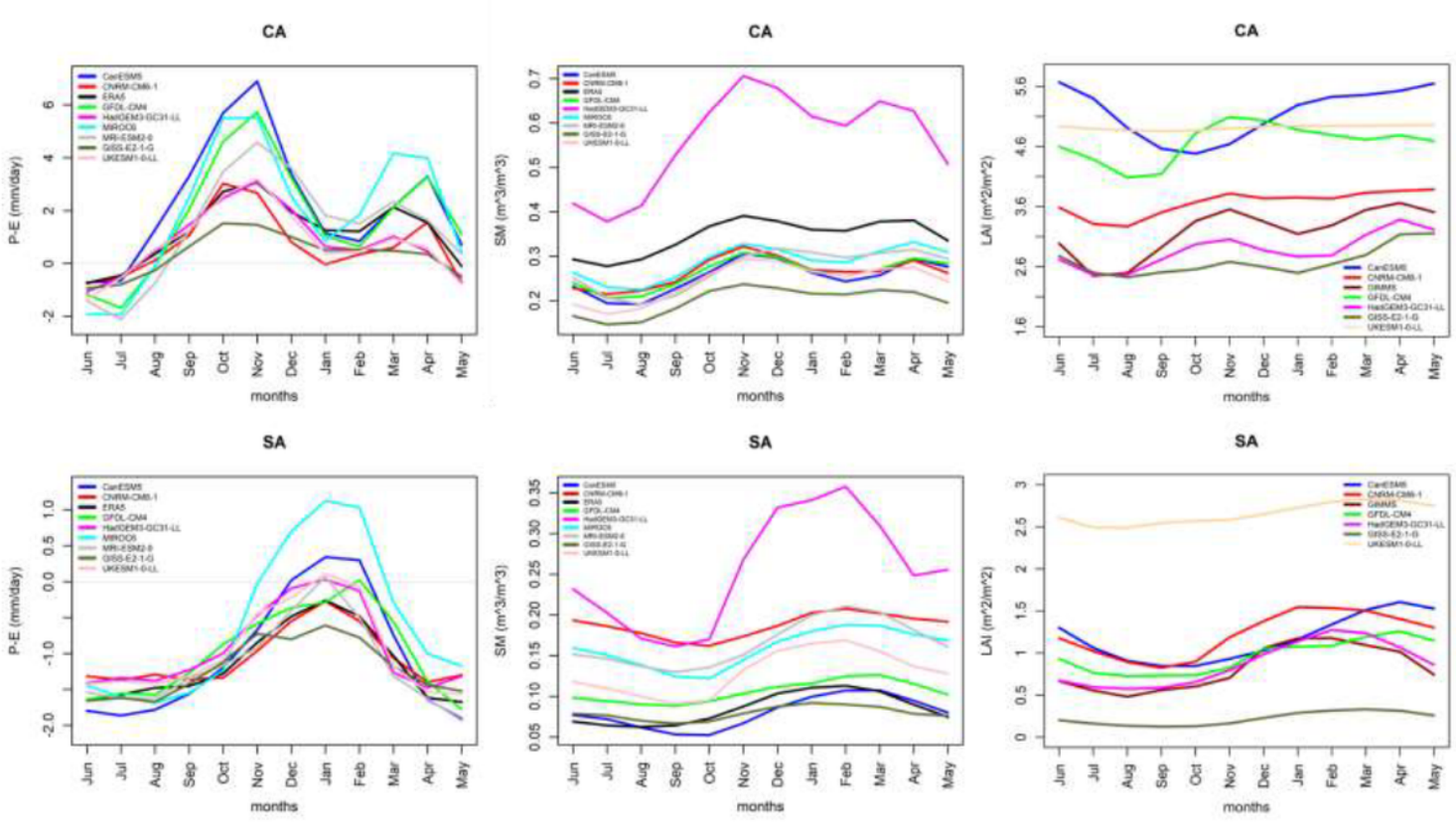

Figure 3

Annual cycle of P-E (left column), SM (middle column) and LAI (right column) over CA (top) and SA (bottom) for ERA5, GIMMS and selected CMIP6 models

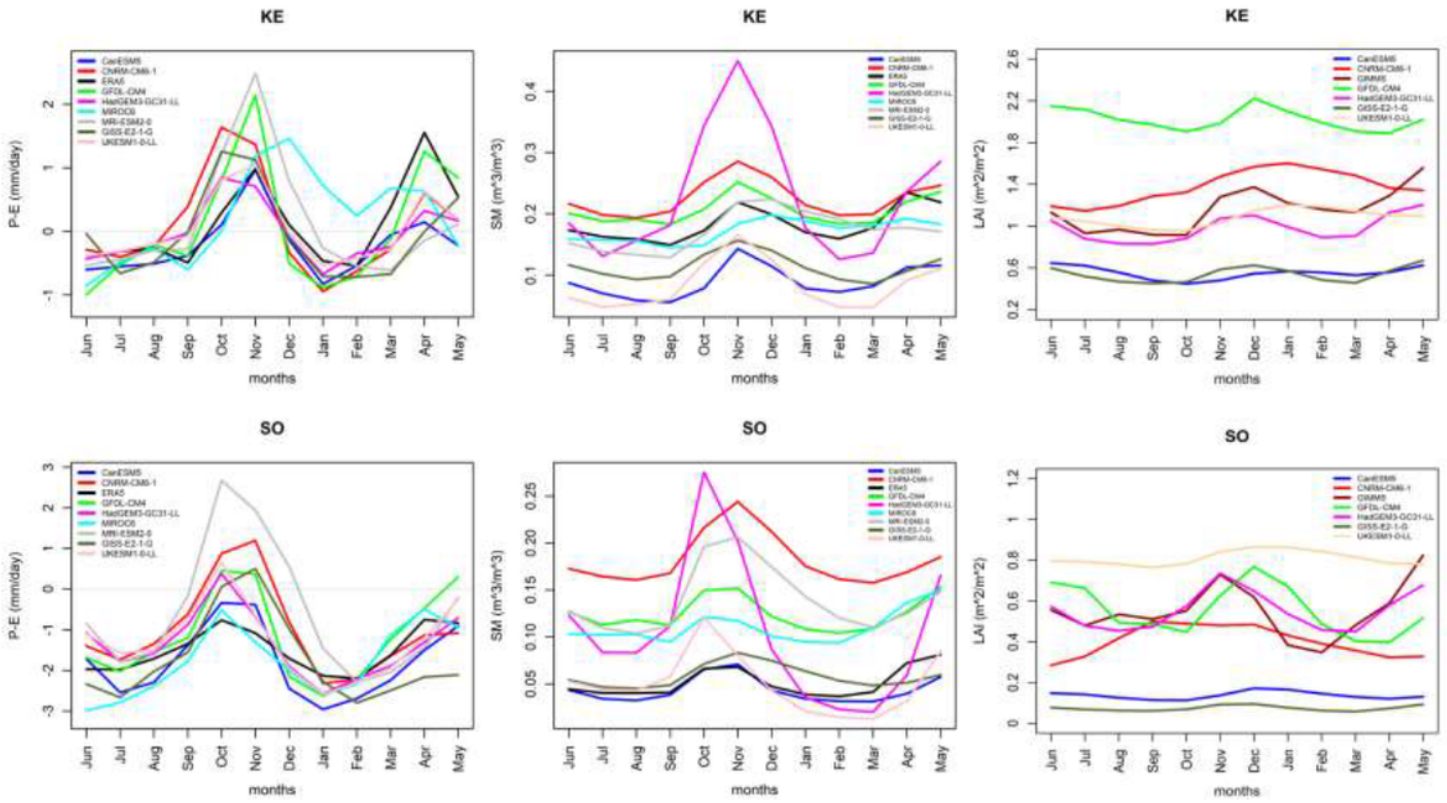

Figure 4

Annual cycle of P-E (left column), SM (middle column) and LAI (right column) over KE (top) and SO (bottom) for ERA5, GIMMS and selected CMIP6 models

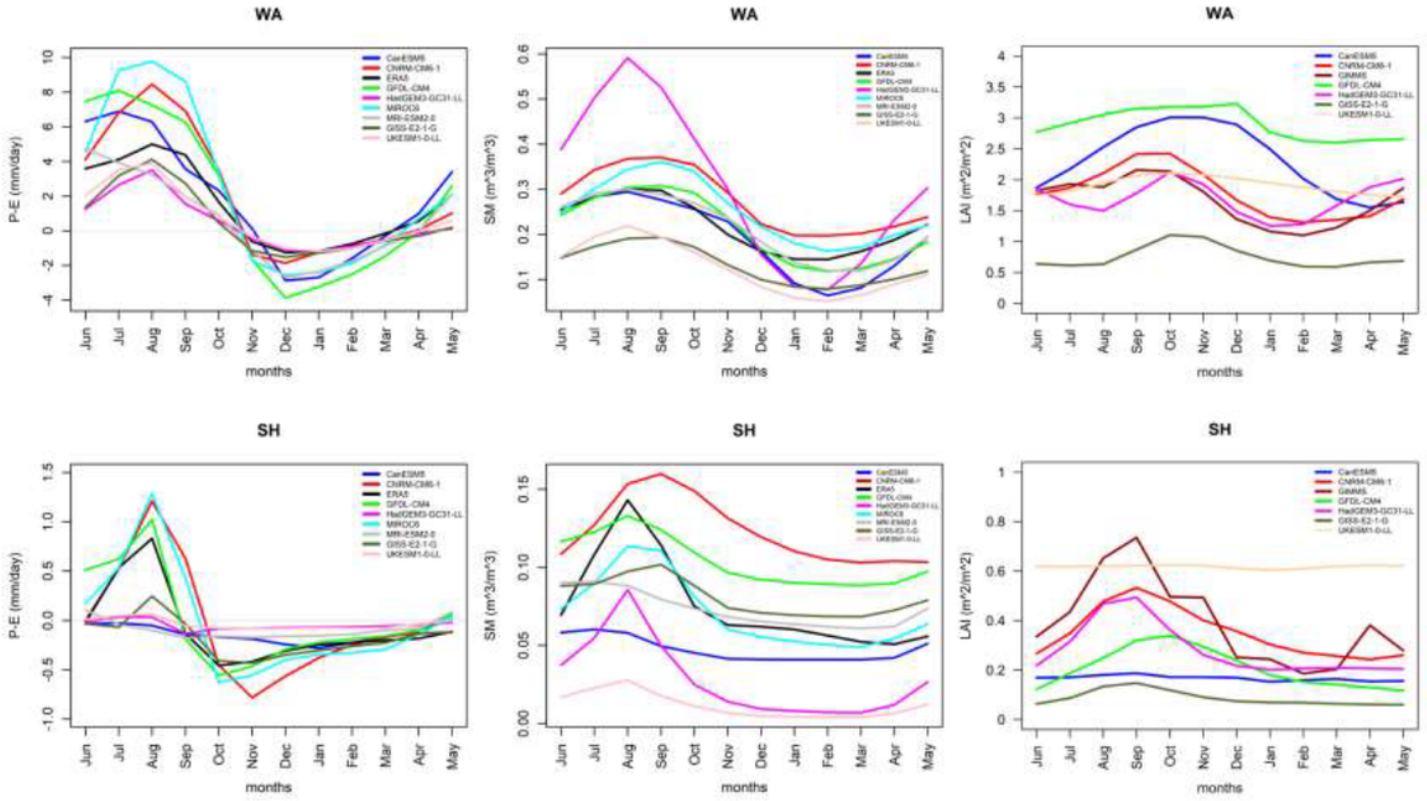

Figure 5

Annual cycle of P-E (left column), SM (middle column) and LAI (right column) over WA (top) and SH (bottom) for ERA5, GIMMS and selected CMIP6 models

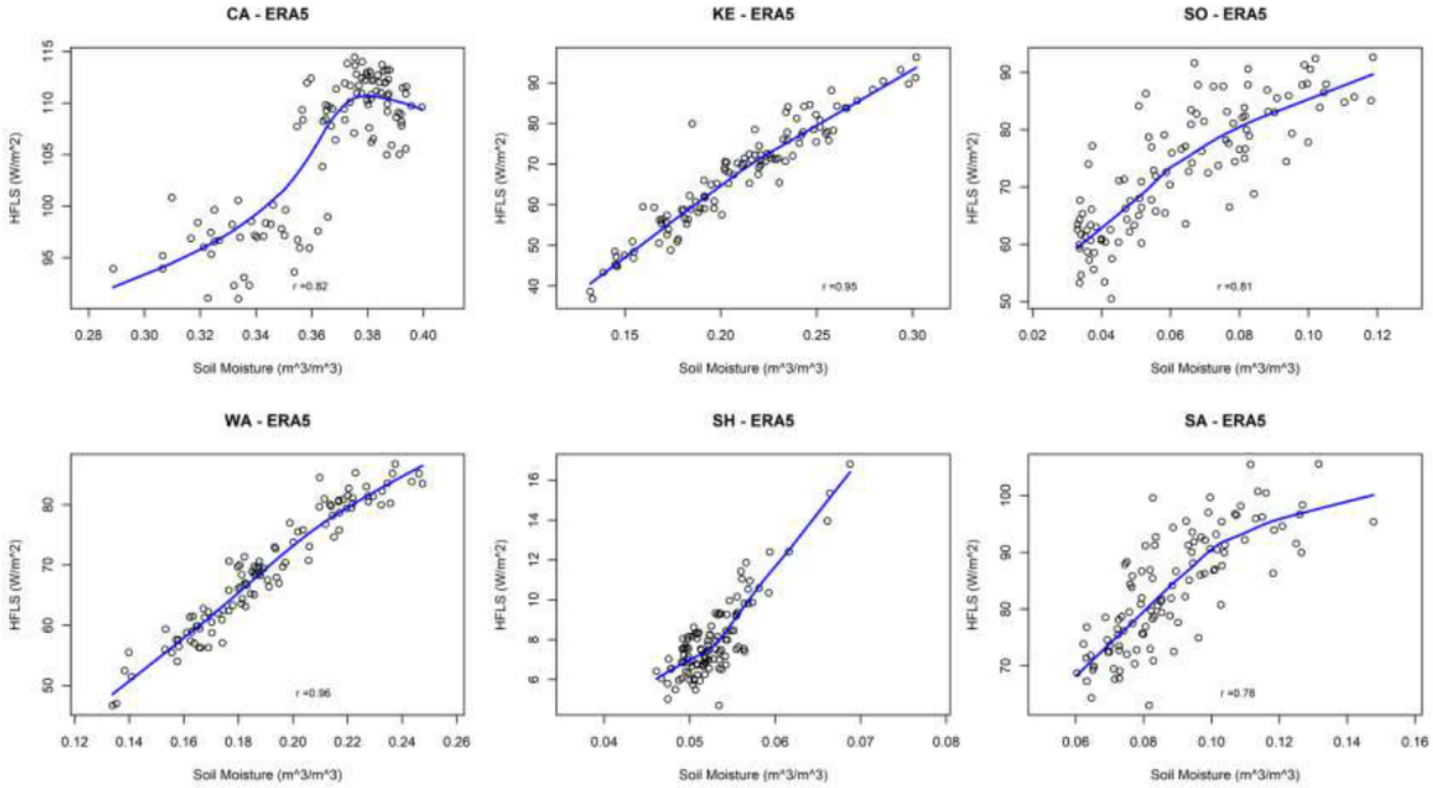

Figure 6

Scatter diagrams for soil moisture and latent heat flux with LOWESS line for study regions over Africa based on ERA5 data for the months of March-May over the period 1979-2014

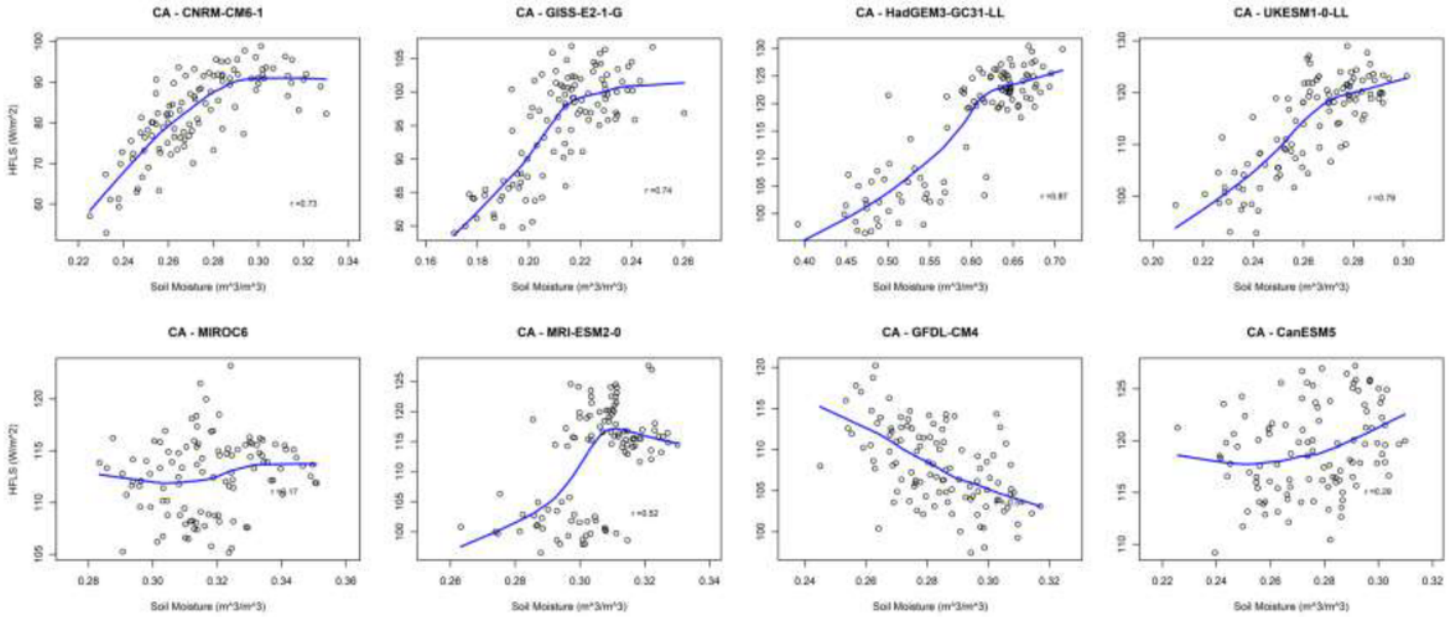

Figure 7

Scatter diagrams for soil moisture and latent heat flux with LOWESS line for study regions over Africa based on ERA5 data for the months of March-May over the period 1979-2014

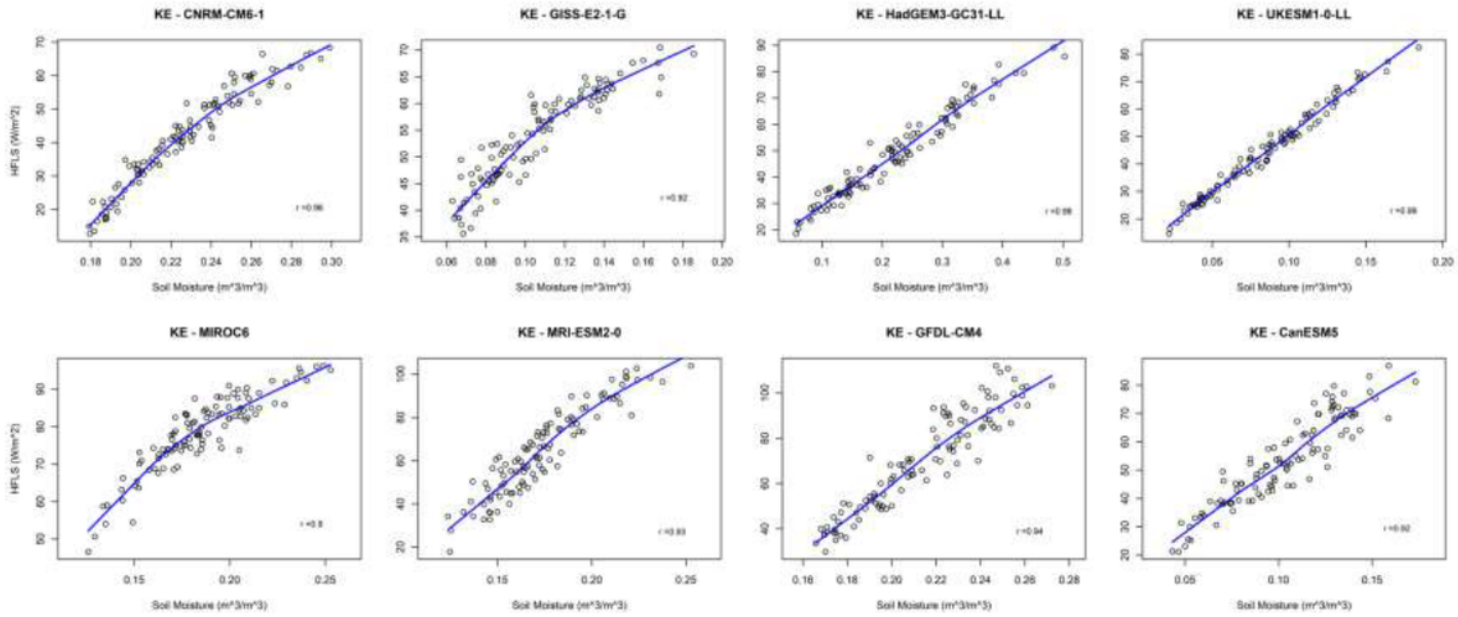

Figure 8

Scatter diagrams for soil moisture and latent heat flux with LOWESS line for study regions over Africa based on ERA5 data for the months of March-May over the period 1979-2014

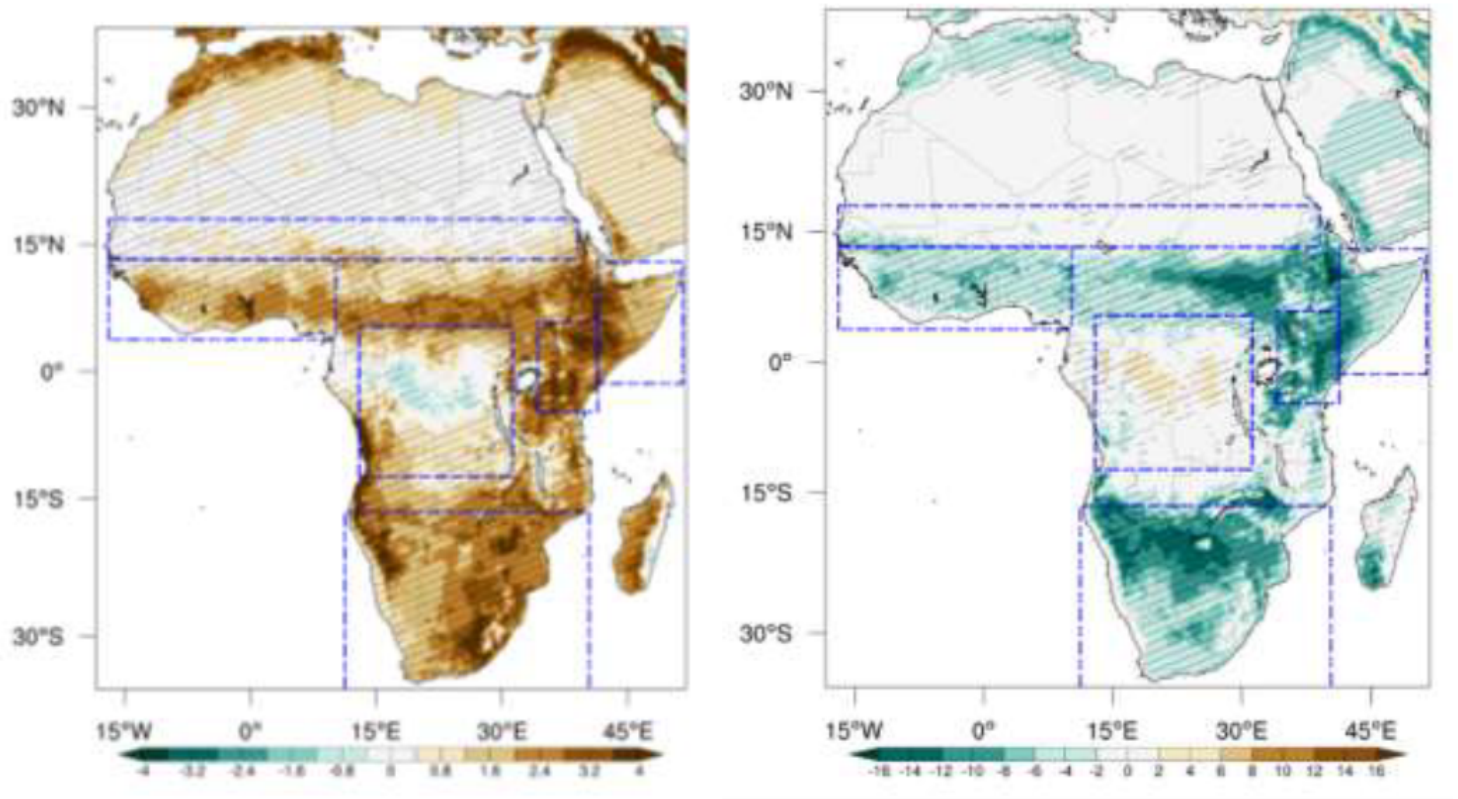

Figure 9

ERA5 MAM seasonal TCI (left) and ACI (right) averaged over the 1974-2014 period. Positive TCI and negative ACI indicate regions of coupling. Brown (green) shades indicate regions of land-atmosphere coupling at different intensities for TCI (ACI). The TCI plot has been scaled by 10^2. Hatching indicates significant correlations.

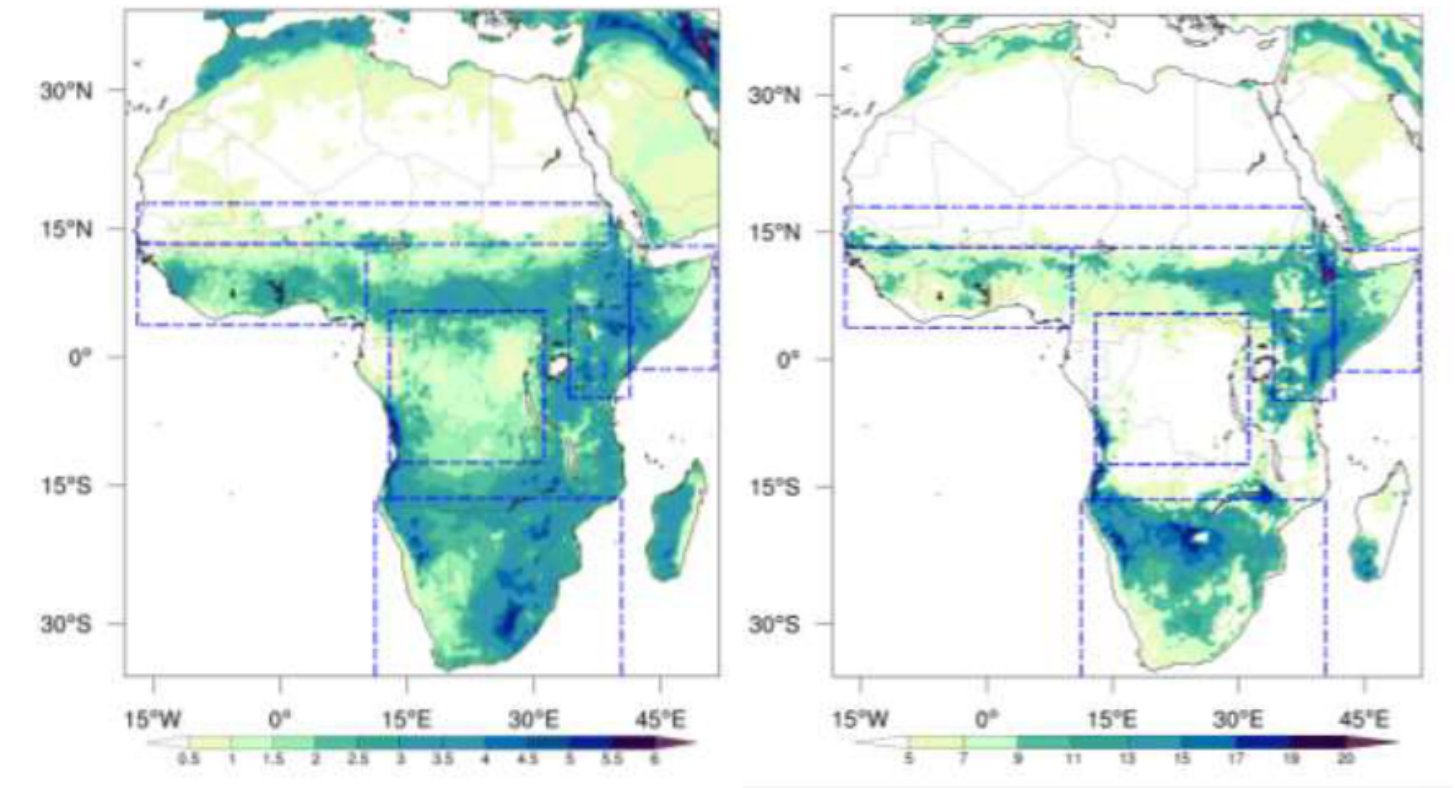

Figure 10

MAM standard deviation for soil moisture (left), scaled by 10^2 and latent heat flux (right) for ERA5 over the period 1979-2014

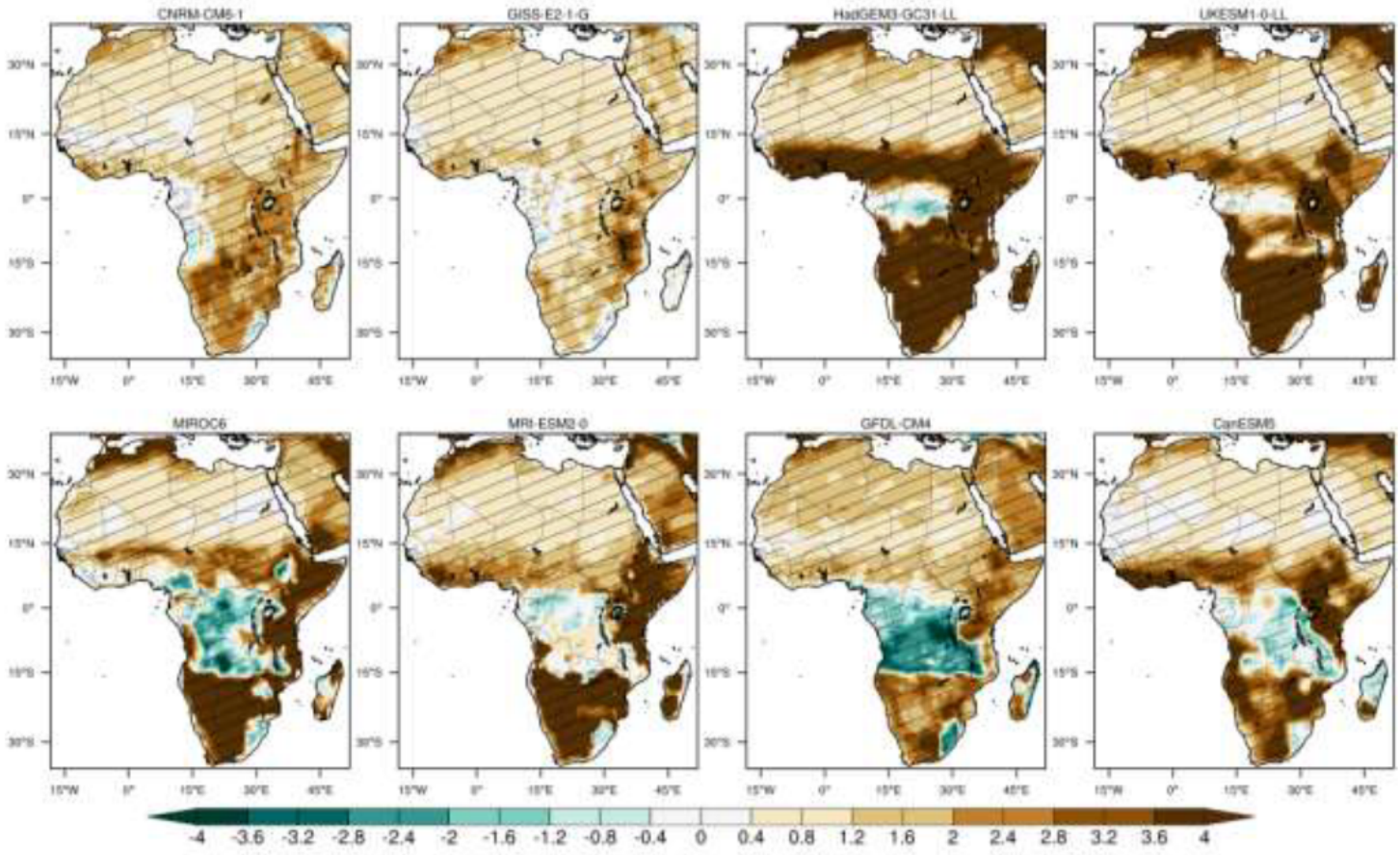

Figure 11

MAM TCI over Africa for selected CMIP6 models for the period 1979-2014 (Brown shades indicate regions of land-atmosphere coupling at different intensities while hatching is used to highlight regions of significant correlations. TCI values scaled by 10^2)

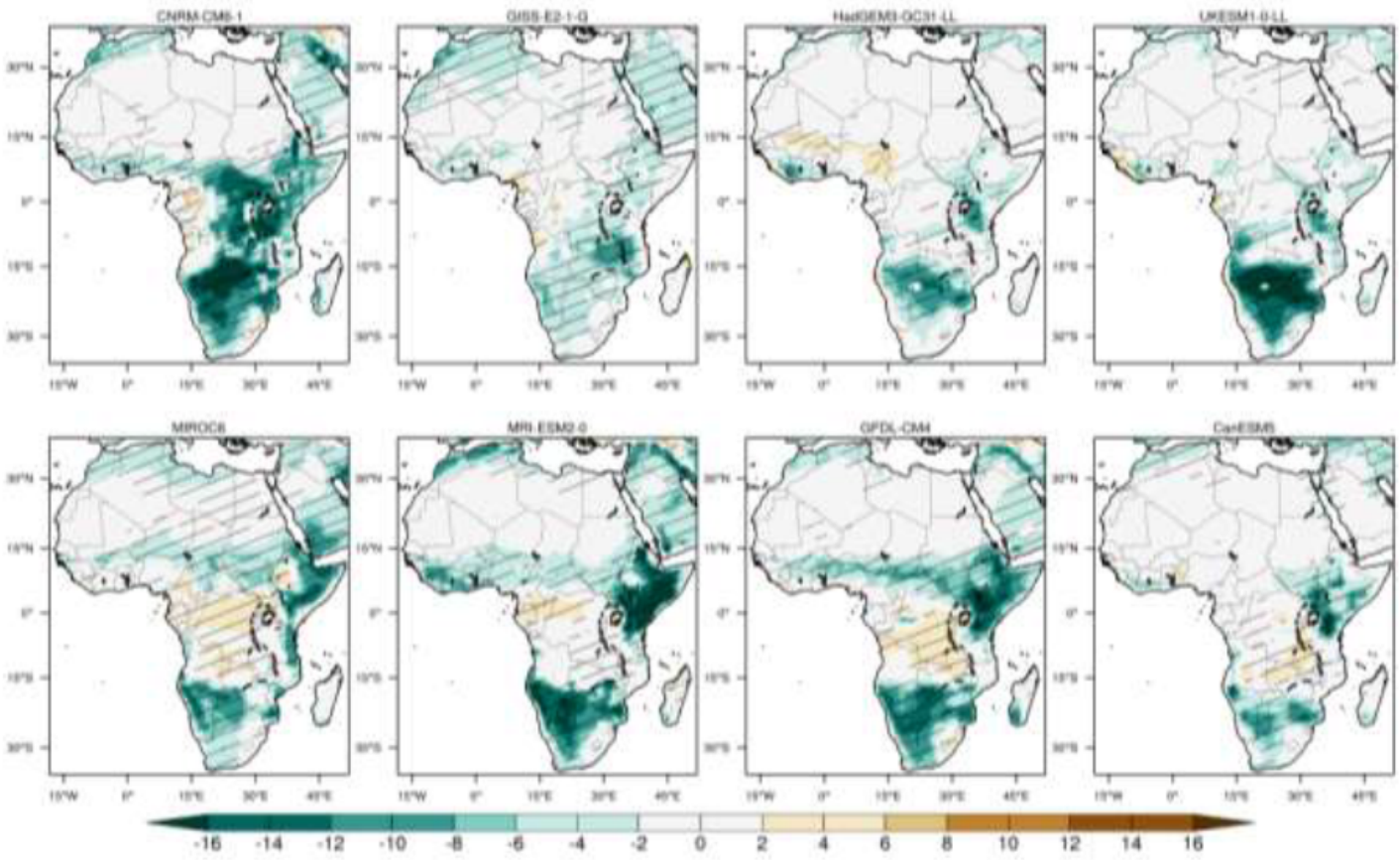

Figure 12

Atmospheric Coupling Index over Africa during MAM season for selected CMIP6 models (Green shades indicate regions of land-atmosphere coupling, at different intensities. Hatching shows regions of significant correlations)

Supplementary Files

This is a list of supplementary files associated with this preprint. Click to download.

- figs1.png
- figs2.png
- figs3.png
- figs4.png
- figs5.png